Journal of
Food Chemistry & Nanotechnology

https://doi.org/10.17756/jfcn.2023-152

Research Article

Open Access

Finite Element Modeling of Bell Pepper Slice Dehydration and Product Characterization on Opto-physico-chemical, Nutritional, and Functional Properties

Rahul Das* and Kamlesh Prasad*

Department of Food Engineering and Technology, Sant Longowal Institute of Engineering & Technology, Longowal, Punjab, India

***Correspondence to:**
Rahul Das
Department of Food Engineering and Technology, Sant Longowal Institute of Engineering & Technology, Longowal, Punjab, India.
E-mail: dasrahul111111@gmail.com

Kamlesh Prasad
Department of Food Engineering and Technology, Sant Longowal Institute of Engineering & Technology, Longowal, Punjab, India.
E-mail: profkprasad@gmail.com

Received: May 04, 2023
Accepted: May 29, 2023
Published: June 02, 2023

Citation: Das R and Prasad K. 2023. Finite Element Modeling of Bell Pepper Slice Dehydration and Product Characterization on Opto-physico-chemical, Nutritional, and Functional Properties. *J Food Chem Nanotechnol* 9(2): 63-77.

Published by United Scientific Group

Abstract

Bell pepper (BP) (*Capsicum annuum* L.) is popularly used as a seasoning ingredient in most breakfasts, supper, snacks, and fritter foods. Three common BP's (green-G, yellow-Y, and red-R) are fascinating to the food technologist to develop even functional food items. Being highly perishable, it is essential to convert them into shelf-stable material, maintaining their physico-chemical, nutritional, optical, functional, and morphological properties. Thus, the effect of hot air drying at 50 to 80 °C at an interval of 10 °C on the quality attributes of GYR-BP was assessed. The dehydration studies were performed for the heat and mass transfer modeling using the finite element method applying the COMSOL Multiphysics 6.0 software. Dehydration behavior was found to be temperature dependent and significantly affected the drying rate and moisture diffusivity. The empirical model Bolbay and Sahin was found to be most appropriate in describing dehydration kinetics. Hot air drying at 60 °C is recommended for the drying of BP. The BP samples dehydrated at 60 °C showed better color retention properties, higher total phenolic and flavonoid content than those dried at different temperatures. Relative crystallinity of freeze-dried samples was found to be lower than optimized samples obtained using hot air drying. The simulated outcomes from the FEM (Finite Element Method) model were found similar to experimental findings, which indicate FEM approach may successfully be applied in predicting heat and mass transfer phenomena in the convective drying. The opto-physico-chemical, nutritional, and functional properties of developed dehydrated shelf stable all types of BP slices were assessed and presented.

Keywords

Bell pepper, Drying, Heat and mass transfer modelling, Color, Antioxidant property

Introduction

The BP is one of the most consumed horticultural crops used as a seasoning ingredient across the globe. According to the data from FAOSTAT in 2021, the global cultivation area of BP was reported to be 2.06 million hectares, with a production volume of 3.63 million metric tons. Fresh BP is cultivated in 126 countries worldwide, with China leading as the largest producer, closely followed by Mexico [1]. They are grown as annual or perennial crops in the field or as greenhouses. They are herbaceous in nature and frost-sensitive crops. Commercially, BP is highly demandable due to its distinctive aroma, pungency, color, and flavor. Nowadays, pepper is gaining popularity because they are free from cholesterol, low in calories, and presents diverse bioactive compounds, including carotenoids, polyphenols, vitamin A, C, E, and alkaloids in high proportion and possesses antimicrobial and antioxidant properties [2-6]. Regular consumption of BP reduces the risk of various ailments such as neurological disorders, rheumatism, lumbago, pharyngitis, arthritis, diabetes, cancer, and cardiovascular diseases [7, 8]. Besides their nutritional and medicinal value, BP are available in various colors (green-G, yellow-Y, and red-R), attracting consumers. Typically, they are used as coloring and flavoring agent in the preparation of paste, pickles, sauces, and pizzas, even consumed fresh in the form of salads [9].

Moreover, it is possibly used as a dried vegetable in bits, granules, or powder to prepare various ready-to-eat fast food items. Fresh BP, rich in nutrients with higher moisture content, are susceptible to heat and rapidly degrades due to microbial spoilage [10]. Therefore, more extended storage is impossible unless or before some preservation techniques (drying, refrigeration, caning, freezing, irradiation, and the addition of chemicals) are imposed. Among the different preservation processes, convective drying is proven to be the simplest processing and preservation techniques that help reduce the required water activity level while maintaining the highest quality attributes [11].

The basic principle of the drying process of any food materials is based on the simultaneous heat and mass transfer with the surrounding air. The process might be translated into a fundamental mathematical model to predict realistic heat and mass transfer mechanisms for describing a system's inherent physics. It accurately estimates foods under complex, realistic conditions, such as variations in initial temperature, regularly shaped geometries, and time-dependent boundary conditions [12]. Researchers have performed numerous mathematical models, fundamental models, and different drying methods for agricultural food products [13-20]. However, limited studies have been observed in the cited literature for the dehydration characteristics and quality attributes of colored BPs. Considering the key gaps, the specific objectives of current research work were to compare convective drying properties and opto-physico-chemical, nutritional, and functional quality attributes of GYR-BP's, to fit available dehydration models to describe thin layer drying kinetics and to develop a 3-dimensional FEM for describing simultaneous heat and mass transfer in convective drying.

Materials and Methods

Raw materials

BPs of different colors were harvested at different stages of maturity. After 15 to 20 days of blossoming, the green fruits were ready for harvest, which begins towards the end of October. In a similar manner, the yellow fruits were harvested after 30 to 40 days of flowering, while the red fruits were harvested after 40 to 50 days. For yellow fruits, harvesting begins after 20th November, while for red fruits, it begins in the middle of December. Three types of fresh sweet BP, Indra - green, Bachata RZ F1 (35-209) - yellow and Massilia RZ F1 - red varieties were procured from the local progressive farmer of Sangrur, Punjab. Attempts have been taken not to harvest the diseased or defective, bruised, and spotted fruits that were discarded from the lot. Only good quality having uniform size, color and maturity were selected. The extraneous matter adhered to the surface samples were removed by keeping the samples under the running tap water. The slices in the form of a disc of an average diameter of 31 ± 0.1 mm were prepared, having a thickness of 3.54 ± 0.16 mm, and used for the convective hot air dehydration experiments.

Proximate analysis

Proximate analysis of BP was determined for moisture, protein, fat, fiber, and ash content (Table 1) using standard method [21].

Table 1: Proximate analysis of three different varieties of BP.

	BP varieties		
Composition	**Green (%)**	**Yellow (%)**	**Red (%)**
Moisture of Fresh BP	93.41 ± 0.24^a	93.21 ± 0.12^a	91.55 ± 0.06^b
Dried BP			
Moisture	7.40 ± 0.20^c	9.54 ± 0.78^b	10.14 ± 0.23^a
Crude protein	8.83 ± 0.57^b	7.59 ± 0.22^c	9.7 ± 0.19^a
Crude fat	1.39 ± 0.29^b	2.94 ± 0.06^a	3.34 ± 0.18^a
Ash	5.67 ± 0.67^b	7.38 ± 0.27^a	5.78 ± 0.51^b
Crude fiber	2.53 ± 0.68^a	3.30 ± 0.23^a	2.53 ± 0.33^a
Carbohydrate	74.18 ± 0.74^a	69.26 ± 0.09^b	68.51 ± 0.17^b

Note: Results are represented as mean ± SD; different letters (a and b) in the same raw are varied significantly at 95% ($p<0.05$) confidence level. Data are represented in wet basis (g/100 g).

Drying experiments

Thin layer convective drying was carried out in a cabinet dryer (Balaji enterprises-48T, Saharanpur, India) at four different temperatures (50, 60, 70, and 80 °C). A freeze-dried sample was prepared using freeze dryer (Lyopfilizer-FD-5, Allied Frost, India) and considered as the reference under the present work. Real-time data for the weight change of sliced disc-shaped BP samples during dehydration was obtained using the precision digital weighing balance attached to the developed dehydration unit [22]. An air circulation having a velocity of 1 m/s was maintained throughout the dehydration experiment. The experimentation was performed separately for 48 h to find the equilibrium moisture content (EMC) at respective temperatures.

Mathematical models for drying kinetics and statistical analysis

Ten thin layer dehydration models have been fitted to see the model efficacy in describing the dehydration kinetics of studied sweet BP slices of different varieties (Table 2). Moisture ratio (MR) and rate of dehydration (R_C) can be calculated by applying Eq. 1 and 2.

$$MR = \frac{M_t - M_e}{M_0 - M_e} \tag{1}$$

$$R_C = \frac{M_t - M_{t+dt}}{dt} \tag{2}$$

Where, M_0, M_e, and M_t are the moisture content of initial, equilibrium, and at any time t. dt is the time interval between two consecutive measurements. The unit of M represents g of water per g of dry solids.

Table 2: Statistical computational results (model parameters, R^2, χ^2, and RMSE) achieved from selected thin layer drying models of GYR-BP slice.

Variety	T (°C)	Models and model parameters	R^2	RMSE	χ^2
Page model $MR = \exp(-kt^n)$					
Green	50	k = 7.98 x 10^{-4} ± 2.6 x 10^{-4}, n = 1.250 ± 0.06	0.988	0.033	1.1 x 10^{-3}
	60	k = 0.003 ± 5.8 x 10^{-4}, n = 1.111 ± 0.033	0.996	0.018	3.1 x 10^{-4}
	70	k = 0.006 ± 5.8 x 10^{-4}, n = 1.152 ± 0.037	0.998	0.015	2.2 x 10^{-4}
	80	k = 0.008 ± 0.002, n = 1.185 ± 0.049	0.998	0.015	2.1 x 10^{-4}
Yellow	50	k = 0.005 ± 5.4 x 10^{-4}, n = 1.025 ± 0.022	0.997	0.015	2.2 x 10^{-4}
	60	k = 0.003 ± 4.3 x 10^{-4}, n = 1.145 ± 0.027	0.998	0.014	1.9 x 10^{-4}
	70	k = 0.006 ± 7.2 x 10^{-4}, n = 1.171 ± 0.027	0.999	0.010	9.7 x 10^{-5}
	80	k = 0.004 ± 0.001, n = 1.284 ± 0.086	0.994	0.028	7.6 x 10^{-4}
Red	50	k = 0.006 ± 3.0 x 10^{-4}, n = 1.008 ± 0.009	0.999	0.006	3.6 x 10^{-5}
	60	k = 0.004 ± 9.8 x 10^{-4}, n = 1.132 ± 0.046	0.993	0.021	4.8 x 10^{-4}
	70	k = 0.004 ± 7.3 x 10^{-4}, n = 1.207 ± 0.039	0.998	0.015	2.3 x 10^{-4}
	80	k = 0.005 ± 8.0 x 10^{-4}, n = 1.240 ± 0.035	0.999	0.011	1.2 x 10^{-4}
Lewis model $MR = \exp(-kt)$					
Green	50	k = 0.003 ± 1.2 x 10^{-4}	0.972	0.051	2.6 x 10^{-3}
	60	k = 0.006 ± 1.4 x 10^{-4}	0.993	0.025	6.2 x 10^{-4}
	70	k = 0.011 ± 3.5 x 10^{-4}	0.994	0.026	6.8 x 10^{-4}
	80	k = 0.018 ± 7.6 x 10^{-4}	0.994	0.029	8.3 x 10^{-4}
Yellow	50	k = 0.005 ± 1.2 x 10^{-5}	0.997	0.015	2.3 x 10^{-4}
	60	k = 0.007 ± 1.4 x 10^{-4}	0.993	0.027	7.1 x 10^{-4}
	70	k = 0.013 ± 3.5 x 10^{-4}	0.994	0.025	6.2 x 10^{-4}
	80	k = 0.014 ± 7.6 x 10^{-4}	0.982	0.047	2.2 x 10^{-3}
Red	50	k = 0.006 ± 3.3 x 10^{-5}	0.999	0.006	3.6 x 10^{-5}
	60	k = 0.008 ± 2.5 x 10^{-4}	0.991	0.029	8.4 x 10^{-4}
	70	k = 0.010 ± 4.1 x 10^{-4}	0.990	0.034	1.0 x 10^{-3}
	80	k = 0.015 ± 6.7 x 10^{-4}	0.991	0.033	1.0 x 10^{-3}
Henderson and Pabis $MR = a\exp(-kt^n)$					
Green	50	a = 0.960 ± 0.023, k = 4.6 x 10^{-4} ± 2.3 x 10^{-4}, n = 1.337 ± 0.085	0.990	0.031	9.5 x 10^{-4}
	60	a = 0.998 ± 0.017, k = 0.003 ± 8.1 x 10^{-4}, n = 1.115 ± 0.045	0.997	0.018	3.3 x 10^{-4}
	70	a = 0.990 ± 0.015, k = 0.005 ± 0.001, n = 1.164 ± 0.045	0.998	0.015	2.3 x 10^{-4}
	80	a = 0.999 ± 0.016, k = 0.008 ± 0.002, n = 1.186 ± 0.058	0.998	0.016	2.5 x 10^{-4}
Yellow	50	a = 0.993 ± 0.013, k = 0.004 ± 7.5 x 10^{-4}, n = 1.035 ± 0.030	0.997	0.015	2.3 x 10^{-4}
	60	a = 0.989 ± 0.013, k = 0.003 ± 5.4 x 10^{-4}, n = 1.162 ± 0.036	0.998	0.014	1.9 x 10^{-4}
	70	a = 0.995 ± 0.010, k = 0.006 ± 8.5 x 10^{-4}, n = 1.177 ± 0.032	0.999	0.010	1.0 x 10^{-4}
	80	a = 0.986 ± 0.028, k = 0.003 ± 0.107, n = 1.306 ± 0.107	0.995	0.029	8.3 x 10^{-4}
Red	50	a = 0.997 ± 0.006, k = 0.006 ± 4.1 x 10^{-4}, n = 1.012 ± 0.012	0.999	0.006	3.7 x 10^{-5}
	60	a = 0.976 ± 0.020, k = 0.003 ± 0.001, n = 1.171 ± 0.059	0.996	0.021	4.6 x 10^{-4}
	70	a = 0.990 ± 0.015, k = 0.004 ± 8.7 x 10^{-4}, n = 1.223 ± 0.05	0.999	0.016	2.4 x 10^{-4}
	80	a = 1.002 ± 0.012, k = 0.005 ± 9.8 x 10^{-4}, n = 1.238 ± 0.04	0.999	0.012	1.4 x 10^{-4}
Logarithmic (Asymptotic) $MR = a\exp(-kt) + c$					
Green	50	a = 1.337 ± 0.025, k = 0.002 ± 7.7 x 10^{-5}, c = -0.347 ± 0.028	0.999	0.010	1.1 x 10^{-4}
	60	a = 1.089 ± 0.015, k = 0.005 ± 2.0 x 10^{-4}, c = -0.083 ± 0.016	0.999	0.013	1.7 x 10^{-4}
	70	a = 1.060 ± 0.014, k = 0.010 ± 3.6 x 10^{-4}, c = -0.054 ± 0.011	0.999	0.014	1.9 x 10^{-4}
	80	a = 1.064 ± 0.020, k = 0.016 ± 7.9 x 10^{-4}, c = -0.056 ± 0.016	0.998	0.017	2.7 x 10^{-4}
Yellow	50	a = 1.021 ± 0.007, k = 0.005 ± 9.7 x 10^{-5}, c = -0.032 ± 0.006	0.999	0.010	1.0 x 10^{-4}
	60	a = 1.096 ± 0.006, k = 0.005 ± 8.3 x 10^{-5}, c = -0.089 ± 0.006	0.999	0.005	2.8 x 10^{-5}
	70	a = 1.052 ± 0.015, k = 0.012 ± 4.3 x 10^{-4}, c = -0.039 ± 0.010	0.998	0.015	2.3 x 10^{-4}
	80	a = 1.103 ± 0.036, k = 0.011 ± 0.001, c = -0.087 ± 0.033	0.993	0.032	1.0 x 10^{-3}

Red	50	a = 1.002 ± 0.005, k = 0.006 ± 7.0 x 10^{-5}, c = -0.002 ± 0.003	0.999	0.006	3.8 x 10^{-5}
	60	a = 1.055 ± 0.017, k = 0.007 ± 3.2 x 10^{-4}, c = -0.058 ± 0.014	0.997	0.019	3.6 x 10^{-4}
	70	a = 1.092 ± 0.015, k = 0.009 ± 3.6 x 10^{-4}, c = -0.080 ± 0.014	0.998	0.014	2.1 x 10^{-4}
	80	a = 1.068 ± 0.026, k = 0.014 ± 8.8 x 10^{-4}, c = -0.046 ± 0.020	0.996	0.024	6.1 x 10^{-4}
Modified page I $MR = \exp\left(-\left(kt\right)^n\right)$					
Green	50	k = 0.003 ± 6.4 x 10^{-5}, n = 1.261 ± 0.049	0.989	0.033	1.1 x 10^{-3}
	60	k = 0.006 ± 9.0 x 10^{-5}, n = 1.113 ± 0.030	0.997	0.018	3.1 x 10^{-4}
	70	k = 0.011 ± 1.8 x 10^{-4}, n = 1.154 ± 0.034	0.998	0.015	2.2 x 10^{-4}
	80	k = 0.017 ± 3.5 x 10^{-4}, n = 1.187 ± 0.045	0.999	0.015	2.1 x 10^{-4}
Yellow	50	k = 0.005 ± 6.4 x 10^{-5}, n = 1.028 ± 0.02	0.997	0.015	2.2 x 10^{-4}
	60	k = 0.006 ± 7.6 x 10^{-5}, n = 1.148 ± 0.024	0.998	0.014	1.9 x 10^{-4}
	70	k = 0.012 ± 1.5 x 10^{-4}, n = 1.172 ± 0.025	0.999	0.010	9.7 x 10^{-5}
	80	k = 0.013 ± 4.0 x 10^{-4}, n = 1.29 ± 0.079	0.994	0.028	7.6 x 10^{-4}
Red	50	k = 0.006 ± 3.5 x 10^{-5}, n = 1.009 ± 0.009	0.999	0.006	3.6 x 10^{-5}
	60	k = 0.008 ± 1.7 x 10^{-4}, n = 1.138 ± 0.042	0.995	0.022	4.8 x 10^{-4}
	70	k = 0.010 ± 1.6 x 10^{-4}, n = 1.211 ± 0.035	0.998	0.015	2.3 x 10^{-4}
	80	k = 0.014 ± 2.0 x 10^{-4}, n = 1.240 ± 0.032	0.999	0.011	1.2 x 10^{-4}
Modified page II $MR = k\exp\left(-t/d^2\right)^n$					
Green	50	k = 1.055 ± 0.036, d = 3.076 ± 13.36, n = 0.034 ± 0.296	0.976	0.049	2.4 x 10^{-3}
	60	k = 1.030 ± 0.020, d = 3.983 ± 10.00, n = 0.099 ± 0.501	0.995	0.024	5.9 x 10^{-4}
	70	k = 1.023 ± 0.026, d = 3.498 ± 10.33, n = 0.142 ± 0.841	0.994	0.027	7.6 x 10^{-4}
	80	k = 1.020 ± 0.032, d = 3.195 ± 13.56, n = 0.186 ± 1.585	0.994	0.033	1.1 x 10^{-3}
Yellow	50	k = 1.005 ± 0.013, d = 4.102 ± 5.18, n = 0.088 ± 0.224	0.997	0.016	2.5 x 10^{-4}
	60	k = 1.033 ± 0.022, d = 3.863 ± 9.90, n = 0.100 ± 0.520	0.994	0.026	6.6 x 10^{-4}
	70	k = 1.025 ± 0.025, d = 3.401 ± 9.43, n = 0.153 ± 0.851	0.994	0.026	6.6 x 10^{-4}
	80	k = 1.034 ± 0.049, d = 3.384 ± 19.90, n = 0.160 ± 1.887	0.983	0.051	3 x 10^{-3}
Red	50	k = 1.001 ± 0.005, d = 4.003 ± 2.01, n = 0.102 ± 0.102	0.999	0.006	3.9 x 10^{-5}
	60	k = 1.018 ± 0.027, d = 3.667 ± 10.66, n = 0.114 ± 0.668	0.992	0.030	9.3 x 10^{-4}
	70	k = 1.035 ± 0.032, d = 3.519 ± 13.02, n = 0.135 ± 1.007	0.991	0.035	1.0 x 10^{-3}
	80	k = 1.034 ± 0.034, d = 3.288 ± 13.15, n = 0.166 ± 1.336	0.992	0.035	1.0 x 10^{-3}
Wang and Singh $MR = 1 + at + bt^2$					
Green	50	a = -0.002 ± 3.2 x 10^{-5}, b = 1.5 x 10^{-6} ± 5.7 x 10^{-8}	0.997	0.017	2.8 x 10^{-4}
	60	a = -0.004 ± 1.0 x 10^{-4}, b = 5.5 x 10^{-6} ± 2.8 x 10^{-7}	0.993	0.026	7.0 x 10^{-4}
	70	a = -0.008 ± 2.2 x 10^{-4}, b = 1.5 x 10^{-5} ± 8.4 x 10^{-7}	0.988	0.037	1.4 x 10^{-3}
	80	a = -0.012 ± 4.4 x 10^{-4}, b = 3.5 x 10^{-5} ± 2.6 x 10^{-6}	0.990	0.039	1.5 x 10^{-3}
Yellow	50	a = -0.004 ± 1.0 x 10^{-4}, b = 3.1 x 10^{-6} ± 1.7 x 10^{-7}	0.968	0.052	3.0 x 10^{-3}
	60	a = -0.005 ± 8.3 x 10^{-5}, b = 6.0 x 10^{-6} ± 2.3 x 10^{-7}	0.995	0.022	4.8 x 10^{-4}
	70	a = -0.008 ± 2.9 x 10^{-4}, b = 1.7 x 10^{-5} ± 1.1 x 10^{-6}	0.980	0.048	2.0 x 10^{-3}
	80	a = -0.009 ± 1.8 x 10^{-4}, b = 2.1 x 10^{-6} ± 8.0 x 10^{-7}	0.996	0.027	4.9 x 10^{-4}
Red	50	a = -0.004 ± 1.3 x 10^{-4}, b = 3.8 x 10^{-6} ± 2.3 x 10^{-7}	0.943	0.068	5.0 x 10^{-3}
	60	a = -0.006 ± 1.4 x 10^{-4}, b = 8.0 x 10^{-6} ± 3.9 x 10^{-7}	0.987	0.037	1.0 x 10^{-3}
	70	a = -0.007 ± 1.5 x 10^{-4}, b = 1.3 x 10^{-5} ± 5.5 x 10^{-7}	0.995	0.025	6.1 x 10^{-4}
	80	a = -0.010 ± 3.7 x 10^{-4}, b = 2.3 x 10^{-5} ± 1.7 x 10^{-6}	0.984	0.046	2.0 x 10^{-3}
Balbay and Sahin $MR = \left(1-a\right)\exp\left(-kt^n\right)+b$					
Green	50	a = -0.0447 ± 0.088, k = 0.002 ± 3.9 x 10^{-4}, n = 0.944 ± 0.038, b = -0.448 ± 0.083	0.999	0.010	1.0 x 10^{-4}
	60	a = -0.100 ± 0.037, k = 0.005 ± 0.001, n = 0.986 ± 0.046, b = -0.092 ± 0.032	0.999	0.012	1.6 x 10^{-4}
	70	a = -0.025 ± 0.018, k = 0.007 ± 0.001, n = 1.088 ± 0.042, b = -0.030 ± 0.012	0.999	0.011	1.3 x 10^{-4}
	80	a =- 0.027 ± 0.020, k = 0.010 ± 0.002, n = 1.115 ± 0.058, b = -0.027 ± 0.015	0.999	0.013	1.6 x 10^{-4}

Yellow	50	a = -0.063 ± 0.013, k = 0.007 ± 7.4 x 10^{-4}, n = 0.924 ± 0.020, b = -0.057 ± 0.009	0.999	0.008	5.7 x 10^{-5}
	60	a = -0.070 ± 0.010, k = 0.005 ± 3.4 x 10^{-4}, n = 1.038 ± 0.016, b = -0.070 ± 0.008	0.999	0.005	2.0 x 10^{-5}
	70	a = -0.012 ± 0.010, k = 0.007 ± 8.4 x 10^{-4}, n = 1.132 ± 0.028, b = -0.015 ± 0.006	0.999	0.008	6.0 x 10^{-5}
	80	a = -0.026 ± 0.039, k = 0.005 ± 0.002, n = 1.210 ± 0.111, b = -0.035 ± 0.026	0.996	0.022	7.0 x 10^{-4}
Red	50	a = 0.003 ± 0.007, k = 0.006 ± 5.0 x 10^{-4}, n = 1.012 ± 0.016, b = -2.4 x 10^{-4} ± 0.003	0.999	0.006	3.9 x 10^{-5}
	60	a = -0.023 ± 0.028, k = 0.005 ± 0.002, n = 1.074 ± 0.061, b = -0.038 ± 0.018	0.997	0.019	3.4 x 10^{-4}
	70	a = -0.037 ± 0.014, k = 0.005 ± 7.7 x 10^{-4}, n = 1.126 ± 0.032, b = -0.040 ± 0.010	0.999	0.009	7.6 x 10^{-5}
	80	a = 0.006 ± 0.016, k = 0.006 ± 0.001, n = 1.220 ± 0.052, b = -0.005 ± 0.009	0.999	0.012	1.5 x 10^{-4}
Two term model $MR = a\exp(-kt) + b\exp(kt)$					
Green	50	a = -0.025 ± 0.002, k = 0.003 ± 6.0 x 10^{-5}, b = 1.026 ± 0.006	0.999	0.011	1.2 x 10^{-4}
	60	a = -0.005± 9.9 x 10^{-4}, k = 0.006 ± 1.27 x 10^{-4}, b = 1.016 ± 0.009	0.999	0.013	1.6 x 10^{-4}
	70	a = -0.001 ± 4.8 x 10^{-4}, k = 0.011 ± 3.7 x 10^{-5}, b = 1.015 ± 0.018	0.997	0.020	4.1 x 10^{-4}
	80	a = 0.000, k = 0.018 ± 0.001, b = 1.019 ± 0.031	0.992	0.033	1.1 x 10^{-3}
Yellow	50	a = -0.001 ± 1.4 x 10^{-4}, k = 0.005 ± 4.8 x 10^{-5}, b = 0.995 ± 0.005	0.999	0.008	6.5 x 10^{-5}
	60	a = 0.000, k = 0.007 ± 2.0 x 10^{-4}, b = 1.033 ± 0.019	0.994	0.026	6.6 x 10^{-4}
	70	a = -4.4 x 10^{-4}, k = 0.013 ± 4.6 x 10^{-4}, b = 1.021 ± 0.010	0.996	0.022	4.8 x 10^{-4}
	80	a = 0.000, k = 0.014 ± 0.001, b = 1.034 ± 0.046	0.983	0.051	3.0 x 10^{-3}
Red	50	a = -3.6 x 10^{-5} ± 4.0 x 10^{-5}, k = 0.006 ± 4.7 x 10^{-5}, b = 1.001 ± 0.005	1.000	0.006	3.8 x 10^{-5}
	60	a = -0.001 ± 5.4 x 10^{-4}, k = 0.008 ± 3.0 x 10^{-4}, b = 1.009 ± 0.020	0.995	0.024	6.0 x 10^{-4}
	70	a = -0.002 ± 8.1 x 10^{-4}, k = 0.010 ± 4.1 x 10^{-4}, b = 1.023 ± 0.020	0.996	0.023	5.5 x 10^{-4}
	80	a = -6.5 x 10^{-4} ± 5.1 x 10^{-4}, k = 0.014 ± 7.8 x 10^{-4}, b = 1.029 ± 0.028	0.994	0.030	9.2 x 10^{-4}
Two term exponential $MR = a\exp(-kt) + (1-a)\exp(kat)$					
Green	50	a = 1.024 ± 0.002, k = 0.003 ± 3.9 x 10^{-5}	0.999	0.011	1.1 x 10^{-4}
	60	a = 1.005 ± 9.3 x 10^{-5}, k = 0.006 ± 9.5 x 10^{-5}	0.998	0.013	1.7 x 10^{-4}
	70	a = 1.001 ± 4.7 x 10^{-4}, k = 0.011 ± 2.9 x 10^{-4}	0.997	0.020	3.9 x 10^{-4}
	80	a = -1.333 ± 0.032, k = 0.009 ± 6.2 x 10^{-4}	0.999	0.013	1.6 x 10^{-4}
Yellow	50	a = 1.001 ± 1.2×10^{-4}, k=0.005±3.5×10^{-5}	0.999	0.007	5.7 x 10^{-5}
	60	a =1.004±6.6×10^{-4}, k=0.006±8.7×10^{-5}	0.999	0.011	1.3 x 10^{-4}
	70	a =1.001±2.8×10^{-4}, k=0.013±3.7×10^{-4}	0.996	0.022	4.9 x 10^{-4}
	80	a =1.002±0.001, k=0.001±7.8×10^{-4}	0.988	0.040	2.0 x 10^{-3}
Red	50	a =1.000±3.8×10^{-5}, k=0.006±3.5×10^{-5}	1.000	0.006	3.6 x 10^{-5}
	60	a =1.001±4.9×10^{-4}, k=0.008±2.2×10^{-4}	0.995	0.024	5.6 x 10^{-4}
	70	a =1.002±8.2×10^{-4}, k=0.010±3.2×10^{-4}	0.996	0.024	5.6 x 10^{-4}
	80	a =1.000±5.5×10^{-4}, k=0.015±6.5×10^{-4}	0.993	0.304	9.3 x 10^{-4}

Note: MR: Moisture ratio; the subscripts a, b, c, d, k, and n are the model parameters; t: Drying time (minutes).

The higher coefficient of multiple determinations (R^2), lower Chi-square (χ^2), and lower root mean square error (RMSE) values were considered to determine the adequacy of the fit for dehydration models. The model was fitted using the graphing and analysis of commercially available statistical analytical software OriginPro 2017 (OriginLab Corporation, Northampton, MA, USA).

Effective diffusivity (Deff) and activation energy (Ea) calculation

One dimensional Fick's second law of gas diffusion model (Eq. 3) describes the effective diffusivity during drying various agricultural materials [23].

$$\frac{\partial M}{\partial t} = D_{eff}\nabla(\nabla M) \tag{3}$$

For more extended drying periods, the diffusion equation for the prepared bell pepper slices can be written as Eq. 4.

$$\ln(MR) = \ln\frac{8}{\pi^2} - \left(\frac{\pi^2 D_{eff}}{4b_0^2}\right)t \tag{4}$$

Effective diffusivity (D_{eff}) values for three varieties of bell pepper slices dehydrated at 50, 60, 70, and 80 °C were determined using Eq. 5.

$$D_{eff} = \frac{4\ b_0^2\ k}{\pi^2} \tag{5}$$

Where, k is the slope obtained using linear regression considering ln (MR) and drying time (t) data having b_0 as half thickness of BP in meter.

Bell pepper powder preparation

The hot air convective dried (HAD) and freeze-dried

(FD) BP were ground using the attrition cold grinding technique and sieved through 60 mesh screens to get coarse powder (Figure 1) and packed in metalized zipper pouches and stored at refrigerated conditions (4 °C) for further analysis.

Color properties

Lightness (L*), redness (a*), yellowness (b*), and total color difference (ΔE) as color parameters of convective and freeze-dried samples were analyzed and compared with the respective fresh BP samples, using the optical sensor fitted Hunter lab colorimeter (Hunter Associates Laboratory Inc., Reston, VA, USA) [24]. Before sample measurements, the instrument was first calibrated using white and black tiles. During color measurements, samples were placed 180° along the horizontal axis through which the light spectrum was coming. However, the sample was located on the reflectance aperture which is fixed with the system. Hence, the distance between the sample and colorimeter was zero.

The total color differences (ΔE) between the fresh and dried (FD and HAD) BP samples were determined using Eq. 6.

$$\Delta E = \sqrt{\left(L^* - L_0^*\right)^2 + \left(a^* - a_0^*\right)^2 + \left(b^* - b_0^*\right)^2} \tag{6}$$

Where, L_0^*, a_0^*, b_0^*; L^*, a^*, b^* are the color parameters of fresh and dried samples, respectively.

In addition, chroma (C^*) and browning index (BI) of fresh and dried samples were calculated using Eq. 7 and Eq. 8, respectively.

$$C^* = \sqrt{a^{*2} + b^{*2}} \tag{7}$$

Where, C^* signifies color saturation.

$$BI = \frac{100}{0.17}\left(\frac{a^* + 1.75L^*}{5.645L^* + a^* - 3.012b^*} - 0.31\right) \tag{8}$$

The formula of Hue angle depends on which quadrant the color is located. When "a" has a negative value, "b" has a positive value, the color is located in quadrant II. So, the hue angle (H^*) formula is written as:

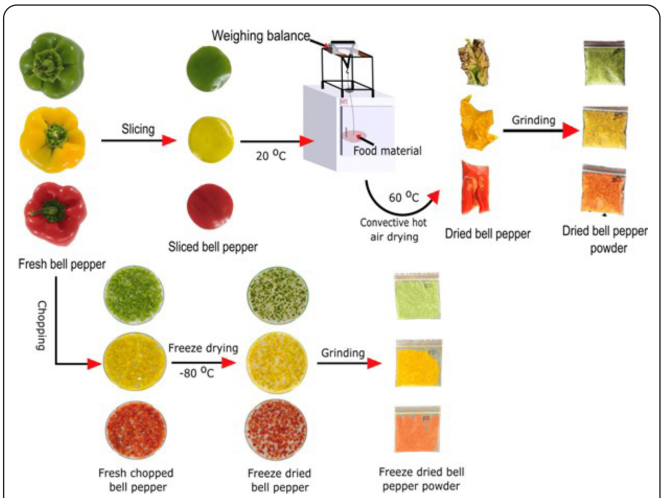

Figure 1: Schematics of freeze dried and cabinet dried powder preparation.

$$H^* = 180 + \tan^{-1}\left(\frac{b^*}{a^*}\right) \tag{9}$$

Otherwise, it is written as

$$H^* = \tan^{-1}\left(\frac{b^*}{a^*}\right) \tag{10}$$

Where, H^* value varies 0° (pure red), 90° (pure yellow), 180° (pure green), and 270° (pure blue).

Functional properties

Water absorption capacity (WAC) and oil absorption capacity (OAC)

The WACF and OAC were determined following the procedure [25]. In brief, 1 g of dried powder was placed into a pre-weighted a glass tube, which was blended with 10 ml distilled water, and incubated at 25 °C for 30 min in the dark chamber. Further, centrifugation was done at 4000 rpm for 15 min. After decanting the obtained supernatant, gain in the sediment weight was reflected as the WAC (Eq. 11)

$$WAC\ (g/g) = \frac{Weight\ of\ sample\ after\ centrifugation\ (g) - Weight\ of\ sample\ taken\ (g)}{Weight\ of\ sample\ taken\ (g)} \tag{11}$$

Similarly, instead of 10 ml distilled water, the soy oil was used to determine the OAC (Eq. 12).

$$OAC\ (g/g) = \frac{Weight\ of\ sample\ after\ centrifugation\ (g) - Weight\ of\ sample\ taken\ (g)}{Weight\ of\ sample\ taken\ (g)} \tag{12}$$

Total phenolic content (TPC), total flavonoid content (TFC), and antioxidant activity

The TPC, TFC, and free radical scavenging activity (FRSA) of FD-BPP and HAD-BPP were examined with slight modifications according to the method described [26, 29]. In brief, a sample of 0.6 g was transferred in a centrifuge tube, and 15 ml of an 80% methanolic solution (80 ml methanol in 20 ml of distilled water) was added. Subsequently, the solution was incubated in an incubator-shaker at 50 °C and 200 rpm for 1 h to facilitate extraction. Following the incubation, the solution was centrifuged to separate and collect the supernatant.

For TPC analysis, 0.1 ml of supernatant was taken and mixed with 2.5 ml of 10% FC (Folin-Ciocalteu) reagent and 2.0 ml of 7.5% Na_2CO_3 without delay. After that, the mixture was kept in water bath (45 °C) for 40 min and absorbance (765 nm) was recorded by using UV spectrophotometer (UV-2600, Shimadzu, Japan). The TPC value was calculated and presented as the gallic acid equivalent, (GAE)/100 g.

In TFC analysis, 0.5 ml of supernatant was mixed with 0.5 ml of pure CH_3OH and 4 ml of distilled water. Then, 0.3 ml of 5% $NaNO_2$ and 0.3 ml of 10% $AlCl_3$ were added to the mixture and kept for 11 min. Subsequently, the absorbance was measured at a wavelength of 510 nm using the same instrument for TPC analysis. The TFC value was determined as the g of quercetin equivalent, (QE)/100 g.

For the antioxidant activity test, 3.9 mg of fresh DPPH was added in 100 ml of pure CH_3OH. Then, 2 ml of extract was mixed with 3.9 ml of DPPH solution and incubated in a dark room for 30 min. Then, absorbance was taken at 515 nm using above mentioned instruments for TPC and TFC analysis. %DPPH free radical scavenging activity was used as the measure to determine the antioxidant activity [30].

Statistical analysis

The above all the experiments were performed in triplicate, and the results were presented as mean ± standard deviation. The data was analyzed using one-way analysis of variance (ANOVA) in SPSS software. To assess the homogeneity of the data and identify significant differences between conditions, LSD and Duncan's multiple range test were employed with a significance level of $p<0.05$.

Morphological analysis

Scanning electron microscopic (SEM) analysis

The morphological features of HAD and FD powdered samples were studied using SEM (JSM-7610FPlus, JEOL Ltd., Tokyo, Japan). The BP powdered samples were put on a double-sided conductive tape, which was coated with gold, and then moved to the apparatus, where micrographs at different magnifications were recorded.

X-ray diffraction (XRD) pattern

The X-ray diffractometer (XRD, D8 ADVANCE, Bruker, Germany) was used to perform an X-ray analysis of FD-BPP and HAD-BPP samples. Powders were subjected to an X-ray beam in XRD pattern determinations at 30 mA and 40 kV with a wavelength of 1.54 Å to examine the change in crystallinity. Data was documented in a 5 - 50° range with a step angle of 0.05° diffraction angle (2θ). The degree of crystallinity was measured using different patterns produced [31]. The relative crystallinity was calculated using Eq. 13.

$$\%\,\text{Crystallinity} = \frac{\text{Area of Crystalline Peak}}{\text{Area of Crystalline Peak} + \text{Area of Amorphous Peak}} \times 100 \tag{13}$$

Fourier-transform infrared spectroscopy (FTIR) analysis

The FTIR analysis was performed using the spectrophotometer (L1600300 Spectrum, two LIT-a FTIR, UK) to identify the essential functional groups of FD-BPP and HAD-BPP samples. The infrared radiation (IR) ranges from 4000 - 600 cm^{-1} were used to obtain the spectrum information. The background was measured after the cleaning of the attenuated total reflection (ATR) plate.

Development of heat and mass transfer model

During convective drying, food and surrounding air domains exchanges heat and mass. Therefore, simulation of the heat and mass transfer process is important for better insight the actual behaviour of the drying system. In any modelling procedure, the very first step is to describe the underlying physics of the modelling system. In this present research work, a 3-dimensional based FEM model was developed in COMSOL Multiphysics 6.0 software for analyzing the spatial temperature and moisture distribution within the BP slices.

Model assumption

During drying, the basic assumptions that have been made for simplification of heat and mass transfer problem:

a) Heat transfer in the product was governed by conduction and convection only, and radiation heat transfer is neglected.
b) The sample was homogenous, isotropic, and had constant dimensions throughout the drying process.
c) No internal heat generation in the product.
d) Temperature and moisture distribution of the BP samples were uniform throughout.
e) The air distribution is uniform and drying takes place under isothermal conditions.

Governing equation for heat balance

Fourier law of heat conduction is considered as the governing heat balance equation (Eq. 14) [32].

$$\nabla\left(\mathrm{k}\nabla \mathrm{T}\right) = \rho C_p \frac{\partial T}{\partial t} \tag{14}$$

Where, k is thermal conductivity ($Wm^{-1}K^{-1}$), ΔT is temperature gradient (K/m), ρ is density (kg/m^3), and C_p is specific heat ($Jkg^{-1}K^{-1}$) of the sample.

Governing equation for mass balance

It is considered that only by diffusion moisture transport occurs inside the sample. Thus, Fick's second law of gas diffusion (Eq. 15) used for describing the transient moisture distribution within the food sample [15].

$$\frac{\partial c}{\partial t} = \nabla\left(D\nabla c\right) \tag{15}$$

Where, c is moisture concentration (mol/m^3) at any time t, and D is moisture diffusivity (m^2/s).

Initial conditions for heat and mass transfer

It is essential to incorporate the initial condition into the model during the heat transfer process. At the beginning sample was at 25 °C. Therefore, the initial condition for the energy balance equation in terms of initial temperature (T_0) can be written as:

$$T = T_0 \tag{16}$$

The initial condition for the mass balance equation for water transport is given in terms of initial water concentration inside the domain:

$$c = c_0 \tag{17}$$

Boundary conditions for heat and mass transfer

To describe the axial symmetrical boundary, no heat and mass transfer process occurred. Therefore, heat transfer in symmetrical boundary is governed by the following equation.

$$n.\left(k\nabla T\right)=0 \tag{18}$$

Where, n is the outward unit normal vector on the boundary.

At open boundaries, the heat transfer boundary condition is given by Eq. 19 [33].

$$h\left(T_a-T\right)=k_m\left(c_{bulk}-c\right)\lambda_w M_w \tag{19}$$

Where, h indicates convective heat transfer coefficient (W/m^2), and k_m indicates mass transfer coefficient (m/s). c_{bulk} and c are the bulk moisture concentration (mol/m^3) and moisture concentration (mol/m^3) at any time t. In Eq. 20, the term λ_w denotes the latent heat of water evaporation (J/kg) at the surface of the material, which signifies as a function of temperature as follows:

$$\lambda_w = 2.5 \text{ x } 10^6 \text{ x } \left(\frac{647.3-T}{374.15}\right)^{0.3298} \tag{20}$$

The boundary condition for mass transfer during the drying of the BP sample is written as:

$$h\left(T_a-T\right)=\left(c_{bulk}-c\right) \tag{21}$$

Where, T_a is temperature of air (°C/K), and T is sample temperature (°C/K).

Thermophysical properties

The thermophysical properties such as density (ρ), specific heat (C_p), and thermal conductivity (k) of BP slice are required for the simulation of heat and mass transfer process. The compositional based prediction method was used to determine the values of k and C_p whereas density (ρ) was taken as constant for the entire drying process.

Heat and mass transfer coefficient calculations

In this study, the following equations were used to determine the convective heat transfer coefficient (h_T) and mass transfer coefficient (k_m) [34, 35].

$$h_T=\frac{Nu \text{ x } k_a}{d} \tag{22}$$

$$Nu = 0.23 * Re^{0.8} Pr^{0.4} \tag{23}$$

$$Re \quad \frac{\rho_a \text{ x } v_a \text{ x } d}{\mu_a} \tag{24}$$

$$Pr=\frac{\mu_a c_{pa}}{k_a} \tag{25}$$

$$k_m=\frac{h_t}{\rho_b \text{ x } c_{pa} \text{ x } \left(\frac{k_a}{\rho_a \text{ x } c_{pa} \text{ x } D_{ref}}\right)^{2/3}} \tag{26}$$

Where, k_a, d, ρ_a, ρ_b, v_a, μ_a, c_{pa}, and D_{ref} are the thermal conductivity of air (Wm^{-1}K^{-1}), the diameter of the sample (m), the density of air (kg/m^3), the density of BP (kg/m^3), the velocity of air (m/s), dynamic air viscosity (Pa.s), the specific heat of the air (Jkg^{-1}K^{-1}), and water mass diffusivity (m^2/s).

Simulation procedure

The governing equations, various input parameters, and variables were incorporated in COMSOL Multiphysics 6.0 for heat and mass transfer simulation of BP slices. Free triangular mesh with fine element size was created. Then, the computation was done, and the result was obtained with a time step of 30 min.

Results and Discussion

Proximate analysis

The proximate compositions of three different varieties of BP are presented in table 1. The moisture content of the fresh BP sample ranged from 91.55% (RBP) to 93.41% (GBP), and dehydration at 60 °C resulted in a dried mass having EMC in the range of 7.40% (GBP) to 10.14% (RBP). This may be because RBP had the highest crude protein (9.70%) and fat (3.34%) content, while GBP had the lowest amounts, respectively. Moreover, the maximum ash and crude fiber contents were associated with YBP. Minor inter and intra-varietal data variations may be due to the varietal characteristics, location, maturity, and cultivation practices.

Drying kinetics and mathematical modeling

The dehydration curves of GYR-BP slices at four different hot air-drying temperatures from 50 – 80 °C with a regular interval of 10 °C are represented in figure 2. At the initial dehydration phase higher moisture content of BP resulted in higher diffusion of water molecules and thus higher initial drying rates (DR). After that falling rate period was observed before the termination of the drying process on reaching the EMC (Table 1). Water removal was supposed to be more difficult with the progression of drying mainly due to tightly bound water attached to the water-holding components (protein and carbohydrates), resulting in decreased DR. This result correlates with the previous work [7, 36]. Furthermore, increased DR was also noticed at higher drying temperatures. The higher driving force due to the partial water vapor pressure reduction results in rapid moisture transfer and thus reduces the overall drying time.

MR vs. drying time data for GYR-BP at selected dehydration temperatures was fitted to ten thin layer dehydration models to describe the drying kinetics. Estimated model and statistical parameters are presented (Table 2). The value of the coefficient of multiple determinations (R^2) of GYR-BP samples for all the drying temperatures was found to be more than 0.943, suggesting that all the models adequately fit the dehydration data to predict the desired results using the fitted models (Figure 2A). However, the Bolbay and Sahin model was the best fit for GYR-BP samples for all the drying temperatures

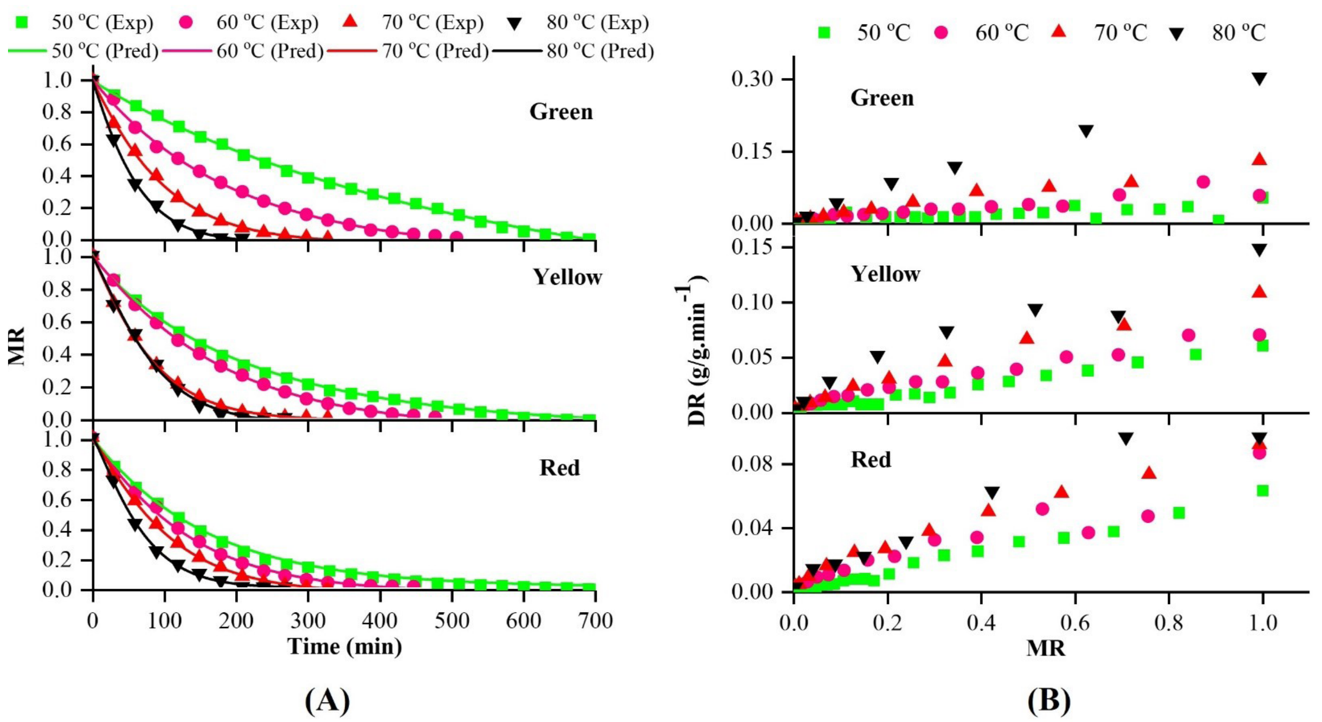

Figure 2: Graphical representation: **(A)** Moisture ratio (MR) of GYR-BP slice at four different hot air-drying temperatures (50, 60, 70, and 80 °C) versus time and **(B)** Drying rate (DR) versus MR of GYR-BP slice at hot air-drying temperatures of 50, 60, 70, and 80 °C.

with higher R^2, reduced χ^2, and RMSE values (Table 2).

Effective moisture diffusivity (Deff) and activation energy (Ea)

The D_{eff} and E_a values of three different varieties of BPs at various hot air-drying temperatures are presented (Table 3). A significant increase in D_{eff} values in the range of 4.44 x 10^{-9} - 2.07 x 10^{-8} m^2/s (GBP), 6.17 x 10^{-9} - 1.78 x 10^{-8} m^2/s (YBP), and 8.48 x 10^{-9} - 3.36 x 10^{-8} m^2/s (RBP) was observed with increase in temperature from 50 – 80 °C and found maximum for RBP variety and found in agreement with the earlier findings [37]. The variation of D_{eff} for GYR-BP samples might be attributed to the variations in the moisture content, composition, structure, variety, and dehydration temperature [38]. In addition, the diffusivity of water created microstructural stress within the sample, indicating material deformation referred to as shrinkage. The measurement of axial and radial shrinkage of GYR-BP samples was quite tricky due to uneven shrinkage during drying. Thus, shrinkage was neglected for modeling

Table 3: Moisture diffusivity (D_{eff}) and activation energy (E_a) of GYR-BP samples at four different hot air-drying temperatures.

	D_{eff} (m^2/s)		
Drying temperature (°C)	**GBP**	**YBP**	**RBP**
50	4.44 x 10^{-9}	6.17 x 10^{-9}	8.48 x 10^{-9}
60	6.88 x 10^{-9}	9.08 x 10^{-9}	1.57 x 10^{-8}
70	1.06 x 10^{-8}	1.24 x 10^{-8}	2.15 x 10^{-8}
80	2.07 x 10^{-8}	1.78 x 10^{-8}	3.36 x 10^{-8}
E_a (kJ/mol)	47.65	33.01	42.23
D_0 (m^2/s)	0.213	0.001	0.060

Note: D_0 is the integration constant.

process to simplify the problem formulations. The E_a for GYR-BP was found to be 47.65 kJ/mol, 33.01 kJ/mol, and 42.23 kJ/mol, respectively, which was varied significantly with the variety. During drying, E_a is the amount of energy required to diffuse the water within the food sample. Found results were in agreement with the earlier reported research findings for drying GBP with E_a of 47.10 kJ/mol [39]. However, the range of 12.87 - 58.15 kJ/mol of E_a was accepted for most food crops [40].

Total phenolic content (TPC), total flavonoid content (TFC), and antioxidant properties

The effect of drying temperatures on antioxidant properties of green bell pepper powder (GBPP), yellow bell pepper powder (YBPP), and red bell pepper powder (RBPP) samples are depicted (Table 4). It can be seen that on increasing the drying temperature from 50 - 60 °C significantly ($p<0.05$) increased the TPC (GBPP: 1431.4 - 1651.3 mg GAE/100 g, YBPP: 1355.3 - 1449.4 mg GAE/100 g, and RBPP: 1479.5 - 1596.6 mg GAE/100 g, respectively) and TFC (GBPP: 581.64 - 621.41 mg GAE/100 g, YBPP: 310.83 - 593.68 mg GAE/100 g, and RBPP: 254.63 - 554.50 mg GAE/100 g, respectively) values. Our findings are consistent with the earlier research [41], which reported a significant increase in TPC by 34.46% (GBP), 75.17% (YBP), and 36.16% (RBP) and TFC by 66.14% (GBP), 139.49% (YBP), and 187.74% (RBP) when the drying temperature was increased from 40 to 60°C. In comparison to FD samples, it was observed that BP samples subjected to 60 °C hot air drying exhibited higher TPC and TFC values. However, maximum TPC and TFC were obtained when samples dehydrated at 60 °C in comparison to all other dried samples. This observation aligns with a similar study [42],

Table 4: Total antioxidant properties of dried BP obtained by freeze drying and hot air-drying methods.

Antioxidant properties	Drying temperature (°C)	GBP	YBP	RBP
TPC (mg GAE/100 g)	FD	1045.3 ± 1.12^{c}	1412.4 ± 1.25^{a}	1390.2 ± 2.06^{b}
	50	1431.4 ± 0.54^{b}	1355.3 ± 0.61^{c}	1479.5 ± 4.10^{a}
	60	1651.3 ± 0.95^{a}	1449.4 ± 2.81^{c}	1596.6 ± 1.73^{b}
	70	1321.0 ± 0.89^{a}	1048.7 ± 3.69^{c}	1228.1 ± 1.79^{b}
	80	1166.2 ± 1.34^{a}	959.0 ± 1.26^{b}	1167.1 ± 2.57^{a}
TFC (mg QE/100 g)	FD	480.61 ± 1.64^{a}	352.02 ± 3.15^{c}	433.52 ± 1.48^{b}
	50	581.64 ± 1.38^{a}	310.83 ± 5.19^{b}	254.63 ± 0.96^{c}
	60	621.41 ± 1.37^{a}	593.68 ± 7.48^{b}	554.50 ± 1.72^{c}
	70	391.02 ± 5.00^{a}	178.13 ± 2.21^{c}	213.81 ± 2.52^{b}
	80	210.21 ± 4.94^{a}	145.52 ± 2.55^{b}	153.34 ± 2.19^{b}
AA (%DPPH)	FD	89.12 ± 1.43^{b}	91.74 ± 0.54^{a}	25.04 ± 0.69^{c}
	50	75.54 ± 0.84^{b}	77.69 ± 0.89^{a}	22.02 ± 0.46^{c}
	60	64.04 ± 1.02^{a}	48.52 ± 1.44^{b}	14.49 ± 0.86^{c}
	70	53.28 ± 0.56^{a}	39.07 ± 2.38^{b}	6.33 ± 0.65^{c}
	80	43.32 ± 2.00^{a}	18.15 ± 1.49^{b}	-

Note: Different letters (a, b, and c) in the same row demonstrated drying conditions that differed significantly ($p<0.05$). TPC: Total phenolic content; TFC: Total flavonoid content; AA: Antioxidant activity; DPPH: 1,1-diphenyl-2-picrylhydrazyl.

who reported that sweet pepper sample dried at 60 °C showed effective retention of bioactive compounds. The observed increase in total phenolic content (TPC) and other considered parameters may be attributed to prolonged dehydration time at lower temperatures and higher thermal exposure at higher temperatures. Additionally, it is possible that the rise in TPC is due to the release of bound phenolic compounds from the cell wall through nonenzymatic interconversion, resulting in the breakdown of esters. [43]. At the same time, the increase in TPC is mainly due to the association of higher enzyme activity to produce flavonoid molecules [44]. Further, decreased TPC and TFC values for GRY-BP samples were observed as temperature increased from 70 – 80 °C. Heat-sensitive antioxidant compounds might be lost due to temperature exposure. Previous research has shown that prolonged periods of dehydration at high temperatures lead to lower-quality products that are linked to enzymatic reactions, caramelization, Maillard reactions, pigment degradation, and vitamin C oxidation, resulting in decreased TFC values [6]. On the other hand, antioxidant activity of natural compounds has been shown to be involved in termination of free radical reactions. The FRSA values for all the GRY-BP samples were temperature dependent and significantly reduced with increasing drying temperature. A possible reason of decreasing FRSA might be due to the presence of reductants, which destroy the free radical and may directly react with the peroxide compounds to prevent further synthesis [45]. However, this result may also be attributed to the decrease in polyphenols, carbonyl, and other compounds due to non-enzymatic browning reactions, intermolecular chemical reactions, and destruction of thermolabile compounds when exposed to high temperatures. Similar findings were also supported by other bell pepper varieties [24]. Overall, the comparison of these results with previously reported studies on bell pepper highlights the influence of drying temperature on the antioxidant properties of bell pepper samples and provides insights into the changes occurring during the drying process.

Color properties

Color is a crucial food quality characteristic that affects consumers taste and acceptance. The color of the BP sample changes on dehydration mainly due to the degradation of chlorophyll content and an increase in carotenoid concentration [19, 46]. The effect of dehydration temperature on color parameters of FD-BPP and HAD-BPP and their respective total color differences (ΔE) (Table 5). The lightness (L^*) values of GBP (65.47), YBP (76.66), and RBP (58.66) at a temperature of 50 °C were found to maximum, followed by a gradual decrease in L^* values with increasing temperature up to 80 °C. The reduction in L^* value may be attributed to the discoloration during dehydration. However, the redness (a^*) value of GBPP was increased from -15.60 to -1.06 with increasing in dehydration temperature from 50 to 80 °C, whereas the yellowness (b^*) value was decreased significantly ($p<0.05$) from 32.15 to 15.24. Besides, the values of a^* for fresh and dried BPP were found negative, representing that they were within the green color space. The decrease in b^* value may be attributed to non-enzymatic reactions and the breakdown of chlorophyll compounds or other pigments [19, 47]. On the other hand, the value of a^* for fresh, FD, and HAD-YBPP did not follow either ascending or descending trends, while b^* decreased with the increased temperature. For HAD-RBPP samples, significant decreased a^* and increased b^* values were observed with increasing temperature. Thus, higher color variation (ΔE) for all the BPP samples was noticed at 80 °C. Furthermore, color saturation (C^*), hue angle (H^*) and browning index (BI) of GYR-BPP were significantly influenced by drying. The C^* and H^* of GY-BPP were decreased with drying temperature. However, C^* values of RBPP did not follow any trend whereas H^* of RBPP was increased with drying temperature. A possible reason for increasing H^* might be due to the formation of brown

Table 5: Color properties of FD-BP and HAD-BP.

BP varieties	Color parameter	Fresh	FD	Drying temperature (°C)			
				50	60	70	80
Green							
	L*	49.85 ± 1.48^{d}	65.47 ± 0.80^{a}	58.59 ± 0.64^{b}	56.33 ± 1.21^{c}	49.19 ± 1.04^{d}	35.36 ± 1.03^{e}
	a*	-21.73 ± 1.23^{e}	-15.60 ± 1.19^{d}	-11.37 ± 0.59^{c}	-9.21 ± 0.21^{b}	-8.15 ± 0.12^{b}	-1.06 ± 0.05^{a}
	b*	21.93 ± 0.79^{c}	32.15 ± 1.51^{a}	24.17 ± 0.88^{b}	22.31 ± 0.45^{c}	18.72 ± 0.96^{d}	15.24 ± 0.35^{e}
	ΔE	-	19.70 ± 1.08^{b}	13.76 ± 0.61^{c}	14.14 ± 0.42^{d}	14.01 ± 0.19^{d}	26.13 ± 0.58^{a}
	C*	30.89 ± 0.78^{b}	35.74 ± 1.81^{a}	26.71 ± 0.98^{c}	24.14 ± 0.35^{d}	20.42 ± 0.85^{e}	15.27 ± 0.35^{f}
	H*	134.71 ± 2.29^{a}	115.86 ± 1.06^{b}	115.19 ± 0.84^{b}	112.44 ± 0.82^{c}	113.57 ± 1.26^{bc}	93.97 ± 0.28^{d}
	BI	16.64 ± 3.94^{d}	44.07 ± 2.31^{b}	35.13 ± 1.40^{c}	35.30 ± 2.03^{c}	32.73 ± 2.83^{c}	52.06 ± 2.10^{a}
Yellow							
	L*	71.40 ± 1.37^{b}	76.66 ± 1.40^{a}	73.00 ± 1.19^{b}	71.48 ± 0.78^{b}	66.16 ± 1.41^{c}	42.49 ± 1.57^{d}
	a*	3.72 ± 0.19^{d}	8.12 ± 0.64^{b}	7.75 ± 0.51^{b}	6.03 ± 0.19^{c}	14.01 ± 0.15^{a}	13.96 ± 0.16^{a}
	b*	60.38 ± 0.67^{a}	61.29 ± 0.79^{a}	59.13 ± 1.01^{a}	54.46 ± 1.14^{b}	47.67 ± 1.89^{c}	37.47 ± 2.08^{d}
	ΔE	-	2.64 ± 0.39^{c}	4.63 ± 1.05^{d}	13.06 ± 0.34^{e}	14.47 ± 2.09^{b}	38.30 ± 2.01^{a}
	C*	60.49 ± 0.67^{a}	61.82 ± 0.82^{a}	59.63 ± 0.98^{a}	54.79 ± 1.14^{b}	49.69 ± 1.79^{c}	39.99 ± 1.98^{d}
	H*	86.48 ± 0.18^{a}	82.46 ± 0.56^{c}	82.53 ± 0.54^{c}	83.68 ± 0.21^{b}	73.61 ± 0.71^{d}	69.54 ± 0.93^{e}
	BI	154.34 ± 7.89^{b}	144.32 ± 4.89^{bc}	147.55 ± 7.28^{bc}	131.82 ± 2.69^{d}	130.84 ± 7.84^{d}	186.77 ± 15.98^{a}
Red							
	L*	48.21 ± 1.07^{b}	58.66 ± 0.56^{a}	54.62 ± 0.39^{b}	54.02 ± 1.93^{b}	37.34 ± 1.30^{c}	33.55 ± 1.17^{d}
	a*	41.24 ± 1.15^{a}	37.81 ± 0.58^{b}	36.80 ± 0.57b	34.28 ± 1.35^{b}	32.93 ± 0.76^{b}	29.01 ± 0.81^{c}
	b*	31.13 ± 1.05^{d}	31.46 ± 1.16^{d}	35.58 ± 1.05^{c}	37.24 ± 0.77^{c}	43.13 ± 0.73^{b}	48.34 ± 1.57^{a}
	ΔE	-	11.04 ± 0.74^{c}	9.00 ± 0.99^{d}	11.04 ± 1.61^{c}	18.24 ± 0.93^{b}	25.76 ± 0.82^{a}
	C*	51.67 ± 1.55^{c}	49.19 ± 0.45^{d}	51.20 ± 0.33^{c}	50.63 ± 0.56^{cd}	54.27 ± 0.18^{b}	56.38 ± 1.76^{a}
	H*	37.04 ± 0.18^{f}	39.75 ± 1.41^{e}	44.03 ± 1.28^{d}	47.38 ± 1.65^{c}	52.64 ± 1.10^{b}	59.03 ± 0.12^{a}
	BI	154.12 ± 5.64^{c}	119.00 ± 2.06^{c}	144.94 ± 3.15^{c}	151.53 ± 5.75^{c}	326.36 ± 18.50^{b}	530.38 ± 29.24^{a}

Note: The superscripts a, b, c, d, and e in the same row represent significant effect ($p<0.05$) on color properties at different drying air temperatures.

pigments at higher temperature. The BI of GY-BPP did not follow any trend and found maximum at 80 °C. In the case of RBPP, the BI was increased with drying temperature. Therefore, all the BP samples dried at 60 °C temperatures resulted in retaining their natural color with higher TPC and TFC, which further prefer for consumer acceptance and suitable for other processing applications.

Water absorption capacity (WAC) and oil absorption capacity (OAC)

The functional properties such as WAC and OAC refer to the amount of water or oil bound by the BPP after applying external force (centrifugal force). The significant variation of WAC and OAC of FD and HAD GYR-BPP at different temperatures are shown in table 6. Drying types and conditions had a significant impact on WAC and OAC. The highest WAC (5.75 g/g) was found with GBP dried at 50 °C. However, a significant reduction in WAC and OAC was observed with the products obtained at increased dehydration temperature. With increasing drying temperatures from 50 to 80 °C, the WAC for YBP and RBP varieties decreased from 20.29% to 35.75% and 7.87% to 42.52%, respectively, when compared to the FD sample. Similarly, in comparison with the FD sample, the trend of OAC for all the BPs decreased from 5.91% to

Table 6: WAC and OAC of dried BP obtained by freeze drying and hot air-drying at different temperatures.

Functional properties	Drying temperature (°C)	GBP	YBP	RBP
WAC (g/g)	FD	3.55±0.02ᵃ	2.54±0.02ᵇ	2.07±0.01ᶜ
	50	5.75±0.01ᵃ	2.34±0.12ᵇ	1.65±0.07ᶜ
	60	4.85±0.03ᵃ	1.90±0.09ᵇ	1.54±0.02ᶜ
	70	4.25±0.05ᵃ	1.71±0.08ᵇ	1.44±0.11ᶜ
	80	3.47±0.20ᵃ	1.46±0.13ᵇ	1.33±0.11ᵇ
OAC (g/g)	FD	1.37±0.01ᵃ	1.52±0.05ᵃᵇ	1.67±0.12ᵃ
	50	1.23±0.02ᶜ	1.36±0.05ᵇ	1.49±0.05ᵃ
	60	1.08±0.03ᵇ	1.24±0.06ᵃ	1.30±0.06ᵃ
	70	0.95±0.01ᵃ	0.84±0.08ᵇ	1.04±0.06ᵃ
	80	0.89±0.04ᵃ	0.71±0.15ᵃ	0.88±0.12ᵃ

Note: For each variety, significant ($p<0.05$) differences between drying conditions were presented with different letters in the same row. Where: FD = freeze drying, WAC = water absorption capacity, and OAC = oil absorption capacity.

20.25%, 6.74% to 29.59%, and 6.35% to 32.14%, respectively, on increasing dehydration temperature. As per the findings of previous research, the water absorption and oil absorption values of pumpkin flour by hot air drying (70 °C) were decreased by 33.43% and 12.44%, respectively, compared to drying at 50 °C [48].

Morphological characteristics

Scanning electron microscopy (SEM)

The SEM is an extremely valuable characterization tool used to obtain detailed images and information about the morphology, size, shape, and organization of the surface topography of various samples. Figure 3A shows the surface morphological characteristics of control (FD) and HAD-BPP samples. A significant change in terms of their shape and surface morphology was observed in HAD samples. No cluster formation was noticed for both FD and HAD samples, indicating that all the samples dried very well. Almost no crakes were present on the surface of the control sample. However, a more irregular shape with a rough surface (surface deformation) was found in HAD samples. These changes may be attributed due to the rapid evaporation of water molecules, changes in internal structure, and generation of higher internal pressure during the convective heating process, which is supported by the findings for green chili powder [49]. On the other hand, the authors have reported that the damage of cellular structure could be alleviated by decreasing the drying temperature [50].

X-ray diffraction (XRD) analysis

The stability of powder is greatly influenced by crystallization, which can be identified using XRD analysis (Figure 3B). The presence of sharp, defined peaks in XRD indicates a crystalline region in which the particles are arranged in a highly ordered state. It is clearly noticed that the least significant variation in the crystalline region between control (FD) and HAD samples, with HAD samples had shown a slightly higher percentage of relative crystallinity (G:41.80%; Y: 40.01%; R: 42.33%). It may be attributed to the release of

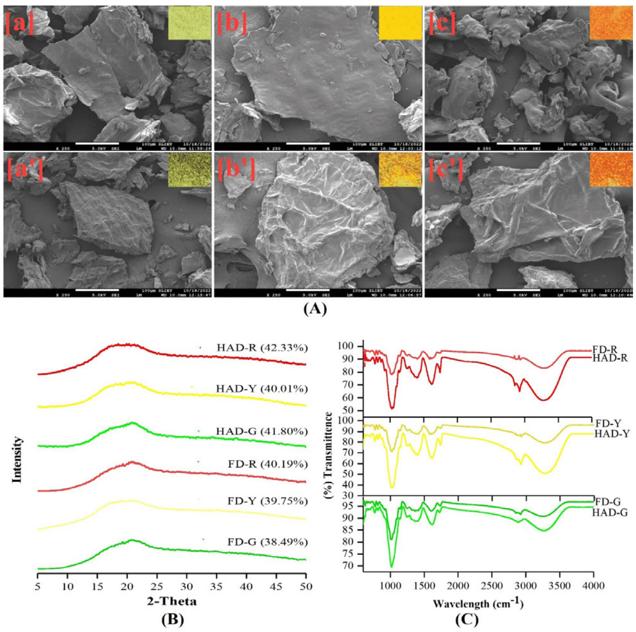

Figure 3: (A) Morphology of bell pepper powder: **(a, b, c)** FD-GYR powders with 250X magnification and **(a', b', c')** HAD (60 °C)-GYR powders with 250X magnification; **(B)** XRD pattern; and **(C)** FTIR analysis of FD and HAD (60 °C) of GYR-BP.

more bioactive compounds and readily available higher O-H groups dried at 60 °C. As the diffraction angle (2θ) increased from 20° to 50°, the diffraction patterns revealed a reduction in peak intensity and noticeable peak shifting, which suggests that the crystalline region had become amorphous due to the destruction of the lamellar portion of starch molecules and double helix structure, breakdown of elongated chain into smaller units, and decrease in polymerization. According to the curve, all the FD and HAD samples had shown a single peak at 20° of diffraction angle, indicates BPP is amphorae materials [51].

Fourier transform infrared spectroscopy (FTIR) analysis

The FTIR spectra and obtained characteristic peaks from the FD and HAD of different varieties of BP are shown in figure 3C. The analysis was done to identify the types of chemical bonds (functional groups such as bioactive compounds, sugars, and vitamins) present in the sample. The data revealed that the first broad stretching band of FD-BPP and HAD-BPP sample was observed at the wavelength of 3288.92 - 3267 cm^{-1}, where there is the stretching vibration of -OH groups. However, the band stretching was found higher in all HAD-BPP samples, representing the existence of higher bioactive phenols and water [52]. The band observed between 2933.61 - 2836.73 cm^{-1} reflects vibration stretching due to aliphatic C-H from the structure of carboxylic acid [53]. The stretching vibration of C=O bonds (esters) was observed at 1744.20 - 1730.69 cm^{-1}, and a peak between 1619.18 - 1604.04 cm^{-1} corresponds to C=C stretching occurring in carotenoids. The C-H bending bands were observed at a wavelength of 1586.55 and 1403.28 cm^{-1} and 1586.51 and 1404.08 cm^{-1} in yellow and red FD samples, respectively. Whereas in YR-HAD sample, it was observed at 1402.92 and 1400.09 cm^{-1}. C-H bending was observed at wavelengths of 1367.93 and 1369.87 cm^{-1} in the FD and HAD of GBP.

The bands observed between 1267.49 and 1145.42 cm^{-1} show the asymmetric C-O stretching in yellow and red FD and HAD samples. It was also reported that the absorption band between 1260 - 1180 cm^{-1} shows the presence of several secondary metabolites. Furthermore, the sharp peak was observed between 1050.15 - 1011.34 cm^{-1} in all the BP varieties, resulting in C-O stretching and the presence of alcohols, phenols, and different saccharide groups such as glucose, sucrose, and fructose [54]. The band at wavelengths 917.47 and 917.04 cm^{-1} reflects the stretching of C-CH and C-OH, which denotes the presence of carbohydrates. Although, peaks obtained below 851.94 cm^{-1} correspond to C-H bonds with aromatic structures. On identifying the FTIR spectra and FD sample of GYR-BP, a slight difference has been observed in the varieties.

Simulated heat transfer profile

The spatial temperature distributions profile of 2D-axiometry and 3D geometry of BP slice drying at 60 °C are presented (Table 7). In the initial condition the temperature of the slice was uniform and in equilibrium with the surrounding temperature, followed by the increased temperature with the dehydration time. The simulated results reveal that the BP slice's surface temperature (T_s) increased rapidly until it reached the wet bulb temperature, slightly higher than the core temperature (T_c) during the initial drying phases. The rapid increase in temperature is mainly due to sudden exposure of the material to the heated air. The moisture evaporation rate was dominant at the surface, resulting in the removal of heat, which prevented the warming up the interior part of slices during initial phase of dehydration. Moisture evaporation rate decreased near the termination of drying period, resulting in an enhanced temperature until it reached the drying air temperature ($T_a = T_c = T_s$) [55]. A Similar trend was found for drying paddy and Ethiopian fresh injera products [56, 57].

Simulated mass transfer profile

The spatial moisture distributions throughout the BP slice (2D-axiometry and 3D-geometry) after exposure to hot air at 60 °C from 0 and 450 min of drying are presented in table 7. Before drying, the moisture distribution across the slices was uniform and in equilibrium with the surrounding air. As the drying started, the surface moisture evaporation rate was increased at the beginning due to the higher temperature and moisture gradient between the slice and surrounding air domain. However, the moisture evaporation rate was higher from the interior part to the product surface, which was then diffused to the surrounding air [58]. In addition, the forms of moisture inside the slice can be divided either in free or combined form. Therefore, the moisture at the surface exists in a free form, which diffuses quickly during the drying process. The intermolecular space of the slice consists of bound moisture, which is strongly bounded with polysaccharides, proteins, and other compounds in the cells, indicating an increased resistance of internal moisture diffusion [59]. Due to the lower diffusing rate, the moisture at the center location was higher than that of the surface until the final phase of dehydration was reached. Similar observations were reported for the drying of carrots [60].

Table 7: Temperature and moisture distribution profiles of BP slice at 60 °C from 0 min and 450 min of drying.

Type of geometry	Temperature profile	Moisture profile
2D-axiyomety	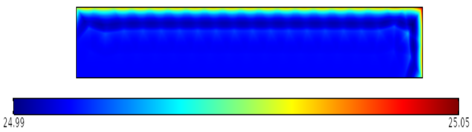	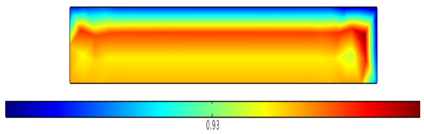
	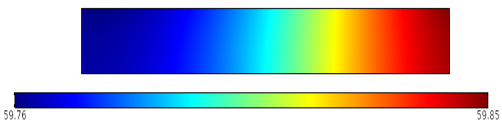	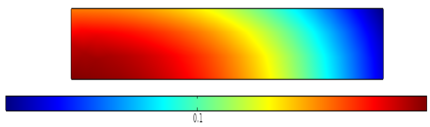
3D	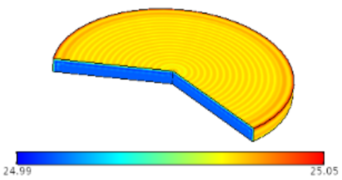	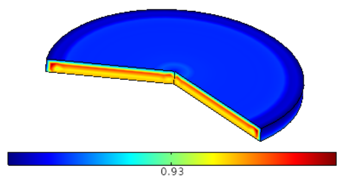
	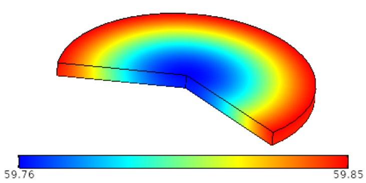	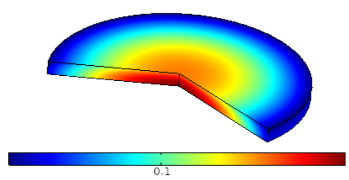

Conclusion

Dehydration of GYR-BP was a temperature dependent phenomenon and affected the effective moisture diffusivity. All fitted mathematical models for the dehydration of GYR-BP showed to predict dehydration characteristics in a better way. However, Bolbay and Sahin model was found to be the best among all. Quality parameters are adversely affected by increasing the temperature above 60 °C. Dehydration at 60 °C also preserved the natural color of BPP with associated chemical, nutrient, functional, TPC, TFC, and antioxidant characteristics, so the product may be suitable for intermediate processed food products to be used in the intended use in making finished food products. The FEM method could be applied successfully to explain and predict heat and mass transfer throughout the convective drying processes.

Acknowledgements

The authors would like to express cordial thanks to Director, Sant Longowal Institute of Engineering and Technology, Longowal, India for extending the support to complete this work.

Funding

The authors would like to express their gratitude to the All-India Council for Technical Education (AICTE), New Delhi, India for providing necessary support as AICTE Doctoral Fellowship (ADF).

Conflict of Interest

There is no conflict of interest among the authors.

References

1. FAOSTAT. 2023. Food and Agriculture Organization of the United Nations. [https://www.fao.org/faostat/en/#data/EP/visualize] [Accessed June 01, 2023]
2. Haq RU, Prasad K. 2017. Antioxidant activity, phenolic, carotenoid and color changes in packaged fresh carrots stored under refrigeration temperature. *Food Measure* 11: 1542-1549. https://doi.org/10.1007/s11694-017-9533-2
3. Kaur R, Prasad K. 2021. Technological, processing and nutritional aspects of chickpea (*Cicer arietinum*)-a review. *Trends Food Sci Technol* 109: 448-463. https://doi.org/10.1016/j.tifs.2021.01.044
4. Kaur R, Shekhar S, Prasad K. 2022. Secondary Metabolites of Fruits and Vegetables with Antioxidant Potential. In Vijayakumar R, Raja SSS (eds) Secondary Metabolites: Trends and Reviews. IntechOpen, pp 141.
5. Sharma R, Joshi VK, Kaushal M. 2015. Effect of pre-treatments and drying methods on quality attributes of sweet bell-pepper (*Capsicum annum*) powder. *J Food Sci Technol* 52: 3433-3439. https://doi.org/10.1007/s13197-014-1374-y
6. Yang XH, Deng LZ, Mujumdar AS, Xiao HW, Zhang Q, et al. 2018. Evolution and modeling of colour changes of red pepper (*Capsicum annuum* L.) during hot air drying. *J Food Eng* 231: 101-108. https://doi.org/10.1016/j.jfoodeng.2018.03.013
7. Arslan D, Özcan MM. 2011. Dehydration of red bell-pepper (*Capsicum annuum* L.): change in drying behavior, colour and antioxidant content. *Food Bioprod Process* 89(4): 504-513. https://doi.org/10.1016/j.fbp.2010.09.009
8. Singh R, Prasad KK, Siddiqui MW, Prasad K. 2017. Medicinal Plants in Preventive and Curative Roles for Various Ailments. In Siddiqui MW, Prasad K (eds) Plant Secondary Metabolites, Volume One. Apple Academic Press, pp 83-120.
9. Pernezny K, Roberts PD, Murphy JF, Goldberg NP. 2003. Compendium of Pepper Diseases. The American Phytopathological Society (APS), St. Paul, MN, USA.
10. Huang LL, Zhang M. 2012. Trends in development of dried vegetable products as snacks. *Drying Technol* 30(5): 448-461. https://doi.org/10.1080/07373937.2011.644648
11. Deng LZ, Mujumdar AS, Zhang Q, Yang XH, Wang J, et al. 2019. Chemical and physical pretreatments of fruits and vegetables: effects on drying characteristics and quality attributes–a comprehensive review. *Crit Rev Food Sci Nutr* 59(9): 1408-1432. https://doi.org/10.1080/10408398.2017.1409192
12. Puri VM, Anantheswaran RC. 1993. The finite-element method in food processing: a review. *J Food Eng* 19(3): 247-274. https://doi.org/10.1016/0260-8774(93)90046-M
13. Khama R. 2022. Mathematical modelling of the solar and convective drying of a thin layer of tomato slices. *Agric Eng Int CIGR J* 24(1): 287-298.
14. Moradi M, Azizi S, Niakousari M, Kamgar S, Khaneghah AM. 2020. Drying of green bell pepper slices using an IR-assisted spouted bed dryer: an assessment of drying kinetics and energy consumption. *Innov Food Sci Emerg Technol* 60: 102280. https://doi.org/10.1016/j.ifset.2019.102280
15. Rani P, Tripathy PP. 2020. Modelling of moisture migration during convective drying of pineapple slice considering non-isotropic shrinkage and variable transport properties. *J Food Sci Technol* 57: 3748-3761. https://doi.org/10.1007/s13197-020-04407-4
16. Singh Y, Yadav P, Yadav YK, Kumar D, Prasad K. 2013. Drying: An Approach Towards Food Preservation. In Kumar S, Yadav PH, Kumar D (eds) Emerging Science and Technology for Food, Agriculture and Environment. Agrobios, Jodhpur, India, pp 441-450.
17. Yadav YS, Prasad K. 2017. Development and characterization of shelf stable quick cooking carrot. *Int Food Res J* 24(1): 465-470.
18. Ankita PK, Prasad K. 2015. Chemical and physical characterization of dehydrated functional fenugreek leaf powder. *Asian J Chem* 27(10): 3697. https://doi.org/10.14233/ajchem.2015.18927
19. Ankita PK, Prasad K. 2015. Characterization of dehydrated functional fractional radish leaf powder. *Der Pharmacia Lettre* 7(1): 269-279.
20. Singh Y, Prasad K. 2012. Variation in engineering characteristics of *Moringa oleifera* leaf to controlled isothermal exposure. *Annals Biol* 28(2): 140-143.
21. AOAC. 2006. Official Methods of Analysis. 18th Edition, Association of Official Analytical Chemists, Gaithersburgs, MD.
22. Prasad K, Singh Y. 2014. Dehydration and quality characterization of *Moringa oleifera* leaves. In Proceedings of 19th International Drying Symposium, Lyon, France.
23. Crank J. 1979. The Mathematics of Diffusion. Oxford University Press, New York, US.
24. Kheto A, Dhua S, Nema PK, Sharanagat VS. 2021. Influence of drying temperature on quality attributes of bell pepper (*Capsicum annuum* L.): drying kinetics and modeling, rehydration, color, and antioxidant analysis. *J Food Process Eng* 44(11): e13880. https://doi.org/10.1111/jfpe.13880
25. Kaur R, Prasad K. 2022. Elucidation of chickpea hydration, effect of soaking temperature, and extent of germination on characteristics of malted flour. *J Food Sci* 87(5): 2197-2210. https://doi.org/10.1111/1750-3841.16147
26. Christ B, Müller K. 1960. For serial determination of the content of flavonol derivatives in drugs. *Arch Pharm* 293:1033-1042. https://doi.org/10.1002/ardp.19602931202

27. Mellors Aa, Tappel A. 1966. The inhibition of mitochondrial peroxidation by ubiquinone and ubiquinol. *J Biol Chem* 241:4353-6. https://doi.org/10.1016/S0021-9258(18)99728-0
28. Singleton VL, Rossi JA. 1965. Colorimetry of total phenolics with phosphomolybdic-phosphotungstic acid reagents. *Am J Enol Viticult* 16:144-158. https://doi.org/10.5344/ajev.1965.16.3.144
29. Téllez-Pérez C, Cardador-Martínez A, Mounir S, Montejano-Gaitán JG, Sobolik V, et al. 2013. Effect of instant controlled pressure drop process coupled to drying and freezing on antioxidant activity of green "Poblano" pepper (*Capsicum annuum* L.). *Food Nutr Sci* 4:321. http://dx.doi.org/10.4236/fns.2013.43043
30. Deng LZ, Yang XH, Mujumdar AS, Zhao JH, Wang D, et al. 2018. Red pepper (*Capsicum annuum* L.) drying: effects of different drying methods on drying kinetics, physicochemical properties, antioxidant capacity, and microstructure. *Drying Technol* 36(8): 893-907. https://doi.org/10.1080/07373937.2017.1361439
31. Nara S, Komiya TJSS. 1983. Studies on the relationship between water-satured state and crystallinity by the diffraction method for moistened potato starch. *Starch* 35(12): 407-410. https://doi.org/10.1002/star.19830351202
32. Dhalsamant K, Tripathy PP, Shrivastava SL. 2018. Heat transfer analysis during mixed-mode solar drying of potato cylinders incorporating shrinkage: numerical simulation and experimental validation. *Food Bioprod Process* 109: 107-121. https://doi.org/10.1016/j.fbp.2018.03.005
33. Kumar C, Karim A, Saha S, Joardder MUH, Brown R, et al. 2012. Multiphysics modelling of convective drying of food materials. In Proceedings of the Global Engineering, Science and Technology Conference, Global Institute of Science and Technology (GIST), Australia.
34. Earle RL. 1983. Unit Operations in Food Processing. Elsevier.
35. Yu XL, Zielinska M, Ju HY, Mujumdar AS, Duan X, et al. 2020. Multistage relative humidity control strategy enhances energy and exergy efficiency of convective drying of carrot cubes. *Int J Heat Mass Transf* 149: 119231. https://doi.org/10.1016/j.ijheatmasstransfer.2019.119231
36. Tunde-Akintunde TY, Afolabi TJ, Akintunde BO. 2005. Influence of drying methods on drying of bell-pepper (*Capsicum annuum*). *J Food Eng* 68(4): 439-442. https://doi.org/10.1016/j.jfoodeng.2004.06.021
37. Vega A, Fito P, Andrés A, Lemus R. 2007. Mathematical modeling of hot-air drying kinetics of red bell pepper (var. Lamuyo). *J Food Eng* 79(4): 1460-1466. https://doi.org/10.1016/j.jfoodeng.2006.04.028
38. Haq RU, Kumar P, Prasad K. 2018. Effect of microwave treatment on dehydration kinetics and moisture diffusivity of Asiatic Himalayan black carrot. *J Saudi Soc Agric Sci* 17(4): 463-470. https://doi.org/10.1016/j.jssas.2016.11.004
39. Faustino JMF, Barroca MJ, Guiné RPF. 2007. Study of the drying kinetics of green bell pepper and chemical characterization. *Food Bioprod Process* 85(3): 163-170. https://doi.org/10.1205/fbp07009
40. Senadeera W, Bhandari BR, Young G, Wijesinghe B. 2003. Influence of shapes of selected vegetable materials on drying kinetics during fluidized bed drying. *J Food Eng* 58(3): 277-283. https://doi.org/10.1016/S0260-8774(02)00386-2
41. Kheto A, Joseph D, Islam M, Dhua S, Das R, et al. 2022. Microwave roasting induced structural, morphological, antioxidant, and functional attributes of Quinoa (*Chenopodium quinoa* Willd). *J Food Process Preserv* 46(5): e16595. https://doi.org/10.1111/jfpp.16595
42. Kaur R, Kaur K, Ahluwalia P. 2020. Effect of drying temperatures and storage on chemical and bioactive attributes of dried tomato and sweet pepper. *LWT-Food Sci Technol* 117:108604. https://doi.org/10.1016/j.lwt.2019.108604
43. Vega-Gálvez A, Di Scala K, Rodríguez K, Lemus-Mondaca R, Miranda M, et al. 2009. Effect of air-drying temperature on physico-chemical properties, antioxidant capacity, colour and total phenolic content of red pepper (*Capsicum annuum*, L. var. Hungarian). *Food Chem* 117(4): 647-653. https://doi.org/10.1016/j.foodchem.2009.04.066
44. Yang W, Du H, Mariga AM, Pei F, Ma N, et al. 2017. Hot air drying process promotes lignification of *Lentinus edodes*. *LWT* 84: 726-732. https://doi.org/10.1016/j.lwt.2017.06.039
45. Tekin ZH, Baslar M. 2018. The effect of ultrasound-assisted vacuum drying on the drying rate and quality of red peppers. *J Therm Anal Calorim* 132: 1131-1143. https://doi.org/10.1007/s10973-018-6991-7
46. Prasad K. 2015. Non-destructive Quality Analysis of Fruits. In Ahmad MS, Siddiqui MW (eds) Postharvest Quality Assurance of Fruits: Practical Approaches for Developing Countries, Springer, Cham, pp 239-258.
47. Ozgur M, Ozcan T, Akpinar-Bayizit A, Yilmaz-Ersan L. 2011. Functional compounds and antioxidant properties of dried green and red peppers. *African J Agric Res* 6(25): 5638-5644. https://doi.org/10.5897/AJAR11.709
48. Roongruangsri W, Bronlund JE. 2016. Effect of air-drying temperature on physico-chemical, powder properties and sorption characteristics of pumpkin powders. *Int Food Res J* 23(3): 962-972.
49. Muneer AS, Al-Dalali S, Al Eryani H. 2018. Microscopic characterizations of green chilli powder. *Int J Curr Microbiol App Sci* 7(8): 2488-2497. https://doi.org/10.20546/ijcmas.2018.708.252
50. Vega-Gálvez A, Lemus-Mondaca R, Bilbao-Sáinz C, Fito P, Andrés A. 2008. Effect of air drying temperature on the quality of rehydrated dried red bell pepper (var. Lamuyo). *J Food Eng* 85(1): 42-50. https://doi.org/10.1016/j.jfoodeng.2007.06.032
51. Zhao X, Zhu H, Zhang B, Chen J, Ao Q, et al. 2015. XRD, SEM, and XPS analysis of soybean protein powders obtained through extraction involving reverse micelles. *J Am Oil Chem Soc* 92: 975-983. https://doi.org/10.1007/s11746-015-2657-9
52. Rybak K, Wiktor A, Kaveh M, Dadan M, Witrowa-Rajchert D, et al. 2022. Effect of thermal and non-thermal technologies on kinetics and the main quality parameters of red bell pepper dried with convective and microwave–convective methods. *Molecules* 27(7): 2164. https://doi.org/10.3390/molecules27072164
53. Ciulu-Costinescu F, Neamțu J, Popescu M, Chirigiu L, Simionescu A, et al. 2015. Preliminary analysis of *Capsicum annuum* L. extracts. *Curr Health Sci J* 41(4): 311.
54. Bureau S, Cozzolino D, Clark CJ. 2019. Contributions of Fourier-transform mid infrared (FT-MIR) spectroscopy to the study of fruit and vegetables: a review. *Postharvest Biol Technol* 148: 1-14. https://doi.org/10.1016/j.postharvbio.2018.10.003
55. Kumar C, Joardder MU, Farrell TW, Millar GJ, Karim A. 2018. A porous media transport model for apple drying. *Biosyst Eng*176: 12-25. https://doi.org/10.1016/j.biosystemseng.2018.06.021
56. Solomon AB, Fanta SW, Delele MA, Vanierschot M. 2021. Modeling and simulation of heat and mass transfer in an Ethiopian fresh *injera* drying process. *Heliyon* 7(2): e06201. https://doi.org/10.1016/j.heliyon.2021.e06201
57. Jha A, Tripathy PP. 2021. Optimization of process parameters and numerical modeling of heat and mass transfer during simulated solar drying of paddy. *Comput Electron Agric* 187: 106215. https://doi.org/10.1016/j.compag.2021.106215
58. Datta AK, Sahin S, Sumnu G, Keskin SO. 2007. Porous media characterization of breads baked using novel heating modes. *J Food Eng* 79(1): 106-116. https://doi.org/10.1016/j.jfoodeng.2006.01.046
59. Jin X, Wang C, Bi Q, Liu Z, Zhang Z. 2020. Study on drying characteristics of corn based on 3D model. *IntJ Food Eng* 16(8). https://doi.org/10.1515/ijfe-2019-0320
60. Timoumi S, Mihoubi D, Zagrouba F. 2019. Modelling of moisture content, β-carotene and deformation variation during drying of carrot. *Int J Food Eng* 15(7). https://doi.org/10.1515/ijfe-2018-0155